J Mater Sci (2007) 42:9021–9029
DOI 10.1007/s10853-007-1881-6

The relationship between atomic partitioning and corrosion resistance in the weld-heat affected zone microstructures of UNS S32304 duplex stainless steel

Carlos Mario Garzón · Carlos A. Serna · Sérgio D. Brandi · Antonio J. Ramirez

Received: 7 March 2006 / Accepted: 25 May 2007 / Published online: 20 July 2007

Abstract Wrought material as well as physically simulated welding heat affected zone (HAZ) samples of an UNS S32304 duplex stainless steel were subjected to electrochemical corrosion tests and electron microscopy characterization. An impaired corrosion resistance of the HAZ microstructures compared to the wrought material microstructure was observed. Calphad-based numerical simulation of phase transformations and solute redistribution taking place during welding provided an explanation of the observed corrosion behavior. The poor corrosion resistance of the HAZ microstructures studied was mainly attributed to a decrease in corrosion resistance of ferritic grains after welding, which exhibited lower chromium content than ferritic grains in the wrought material.

Introduction

The welding of duplex stainless steels (DSSs) strongly affects their fine-grained and duplex-balanced ferrite plus austenite microstructure [1–6]. In particular, in the high temperature heat affected zone (HAZ), a coarse microstructure is formed by a high fraction of ferrite, allotrimorphic and Widmanstätten austenite, and extensive chromium nitride precipitation within ferritic grains [1–6]. When this as-welded microstructure is reheated during multipass welding or during post-weld heat treatment, new austenite, called secondary austenite (γ_2), is formed. This γ_2 may grow from preexisting austenite particles (so called primary austenite, γ_1) and is called intergranular γ_2. Another form of γ_2 can be formed by the nucleation and growth of new intragranular γ_2 particles, mostly within the nitride colonies. Nitride distribution will also be modified, with some intragranular nitrides dissolving and/or new nitride precipitation occurring mainly along ferrite/austenite interfaces [2–7].

It has been frequently reported that the DSS HAZ microstructure exhibits impaired corrosion resistance when compared to the wrought material [1–4]. On the other hand, there is no consensus on the origin of this reduction in corrosion resistance or on the role of γ_2 precipitation.

The detrimental effect of intragranular γ_2 precipitation on the localized corrosion resistance of DSSs welded joints has been reported, and this reduced corrosion resistance has been associated with the lower N, Cr, and Mo content of γ_2 when compared to γ_1 [2, 3, 8, 9]. It has also been suggested that the poor corrosion resistance of the HAZ microstructures is mainly associated with chromium depletion around chromium nitrides within ferritic grains [1].

The objective of this investigation was to study the role of alloy element distribution among ferrite, γ_1, and intergranular γ_2 on corrosion resistance of UNS S32304 DSS HAZ microstructures. Thus, both electron microscopy characterization and electrochemical corrosion tests were performed on simulated HAZ microstructures. The as-welded HAZ and

C. M. Garzón · A. J. Ramirez (✉)
Brazilian Synchrotron Light Laboratory, Caixa Postal 6192 - CEP 13083-970 Campinas, SP, Brazil
e-mail: ramirez@lnls.br

Present Address:
C. M. Garzón
Physics Department, National University of Colombia, Avenida Cra. 30 No 45-03, Ciudad Universitaria, Edificio 404, Bogota, Colombia

C. A. Serna · S. D. Brandi
Metallurgical and Materials Engineering Department, University of São Paulo, Av. Prof. Mello Moraes 2463, CEP 05508-900 Sao Paulo, SP, Brazil

reheated-HAZ microstructures were obtained in a Gleeble® thermo-mechanical simulator. In addition, the analysis of the experimental results was supported by thermodynamic and kinetic simulation of the phase transformations taking place during the thermal cycles.

Experimental

A commercially available UNS S32304 duplex stainless steel was subjected to physical simulation to obtain samples with both as-welded HAZ microstructures (ferritization treatments) and reheated (multipass) HAZ microstructures (reheating treatments). The chemical composition of the DSS is shown in Table 1. The ferritization treatments consisted of an isothermal anneal at 1,350 °C for 5 s followed by rapid cooling; the average heating rate was 300 °C·s^{-1} and the cooling rate at 800 °C was 46 °C·s^{-1}. The reheating treatments were applied to prior ferritized samples, and consisted of isothermal heat treatments at 900 or 1,200 °C for 10 s. The heating and cooling conditions for the reheating and ferritization treatments were similar. The physical simulations were performed in a thermo-mechanical simulator *Gleeble® 1500*, using prismatic samples of 6 × 6 × 90 mm. Detailed information about these treatments was presented elsewhere [6, 7].

Microstructural characterization was performed using optical microscopy (OM), scanning electron microscopy (SEM) and transmission electron microscopy (TEM). Detailed microstructural characterization of the simulated samples is presented elsewhere [6, 7]. Metallographic preparation of samples for OM and SEM consisted of abrasive paper grinding followed by diamond paste polishing and a final stage of 0.05 μm colloidal silica polishing. The specimens were electrolytically etched using a 40%-vol HNO_3 aqueous solution at 25 °C, and applying 1.1 V during ~70 s. The SEM analyses were performed using a JEOL JSM 5900 LV microscope as well as a CAMBRIDGE Steroscan-440 microscope coupled with a wavelength-dispersive X-ray spectrometer (XWDS). TEM samples were prepared by jet polishing with a 70%-vol ethyl alcohol, 20%-vol glycerin and 10%-vol perchloric acid ($HClO_4$) solution at –20 °C and 30 V. The TEM analyses were performed using a JEOL JEM 3010 URP microscope coupled with an energy dispersive X-ray spectrometer (XEDS) system.

The pitting corrosion resistance was evaluated by cyclic potentiodynamic polarization experiments carried out at 25 ± 1 °C in a 3.5 wt-% NaCl naturally aerated solution using a potential scan rate of 1 mV·s^{-1}.

The degree of sensitization (DOS) was evaluated through double loop electrochemical potentiokinetic reactivation (DL-EPR) tests. The DOS was measured as the I_r/I_a ratio, where I_r is the maximum value of the anodic current in the reactivation peak and I_a is the maximum value of the anodic current in the activation peak [10]. The DL-EPR tests were performed in a 0.5 M H_2SO_4 + 0.01 M KSCN naturally aerated solution at 30 ± 1 °C, using a potential scan rate of 1 mV·s^{-1}. The scanned potential range was from the corrosion potential up to 500 mV-SCE.

The cyclic polarization and DL-EPR tests were performed using a Princeton Applied Research Potentiostat–Galvanostat 273A. Saturated calomel and platinum electrodes were used as reference and counter electrodes, respectively. Prior to the corrosion tests, the samples were mechanically ground using abrasive paper to 600 mesh final finish. Five tests were performed for each studied condition.

Numerical simulation

The thermodynamics and kinetics assessment of both austenite growth and chromium nitride dissolution and/or precipitation in the HAZ microstructures was performed using the Calphad-based Thermocalc® and Dictra® software [11] along with the Fe-data and Mob2 databases. A detailed analysis of this numerical modeling is presented elsewhere [12] and only the most important features are presented in this work.

The diffusion-controlled growth of a γ (austenite) region into a $\alpha + M_2N$ (ferrite) region (where M_2N is a nitride with two metallic (M) atoms per each nitrogen (N) atom) was simulated. A closed one-dimensional multi-component system and a planar sharp γ/α interface were assumed.

The atomic diffusion in both ferritic matrix and austenitic grains was computed by solving the multicomponent non-steady state atomic diffusion equation 1 [13]. The interface velocity was calculated using the *mobile interface model* [11], which is implemented in Dictra® software. The establishment of the local equilibrium (LE) condition at the migrating γ/α interface was assumed.

Table 1 Chemical composition of the UNS S32304 duplex stainless steel (wt-%)

Fe	Cr	Ni	Mn	Si	Mo	Cu	C	N
Bal.	22.64	4.81	1.53	0.41	0.30	0.33	0.014	0.10

$$J_K = -\sum_{i=1}^{n} L'_{ki} \frac{\partial \mu_i}{\partial z} \quad (1)$$

In Eq. 1, J_K is the flux of the atomic species k; L'_{ki} is a proportionality factor that depends on the mobility of the atomic species; μ_i is the chemical potential for the species in the system; and z is the spatial coordinate.

Nitrides can precipitate or dissolve within the ferritic matrix as function of temperature and local alloying content. This aspect was taken into consideration by using the *diffusion in dispersed systems model* [11], which is also implemented in Dictra® software.

To compute the growth of austenitic grains, the so-called primary austenite (γ_1), during ferritization treatments, it was assumed the prior existence of 1 nm thick gamma nucleus that begins to grow during the cooling stage at 1,200, 1,100, 1,000, or 900 °C. The chemical composition of this gamma nucleus was set at the equilibrium value corresponding to the temperature at which this nucleus begins to grow. However, to compute the growth of secondary austenite (γ_2) during reheating treatments, it was assumed that γ_2 grows over the previously precipitated γ_1 grains. The average γ_1 width was determined by metallographic measurements and its average chemical composition taken from the previously described precipitation simulations. The size and chemical composition of the remnant ferritic regions were established through mass balance computation by calculating the amount of $\alpha + M_2N$ necessary to reach the steel nominal composition.

Results

Microstructure and chemical composition

The previously reported ferrite grain size and γ_1 fraction on ferritized samples were 240 μm and 16 ± 2%-vol, respectively [6]. In addition, the weighted average width of γ_1 grains was ~7 μm.

After numerical simulation of γ_1 precipitation, it was predicted that γ_1 grains grow with negligible substitutional solute partitioning with the matrix. Furthermore, it was observed that the average chemical composition of γ_1 did not change appreciably as the precipitation temperature was varied between 1,200 and 900 °C. Therefore, the average chemical compositions of γ_1 and remnant ferritic regions were obtained from these calculations. The calculated chemical compositions as well as SEM-XWDS measurements are presented in Table 2. One can see that the calculated values are close to the measured ones. The only important difference is the nitrogen content of γ_1. It must be noted that large experimental errors are expected with XWDS measurements of light element such as nitrogen.

Table 2 Chemical analysis (XWDS) and numerical calculations (NC) of the main elements in the ferritic and austenitic grains of a ferritized sample (wt-%)

Phase		Fe	Cr	Ni	C	N
α	XWDS	Bal.	24.0	4.6	N.M	N.M
	NC	Bal.	22.7	4.8	0.009	0.06
γ_1	XWDS	Bal.	23.3	4.9	N.M	0.48
	NC	Bal.	22.4	4.8	0.039	0.31

N.M: Non measurable value (content was lower than the detection limit)

Table 3 presents the Fe, Cr, and Ni weight fraction of nitrides and the ferritic matrix after the ferritization treatments as measured by TEM-XEDS and as determined via computational modeling. Because the chemical composition of the ferrite measured via XWDS-SEM was used as a standard for the XEDS measurement in the TEM, both compositions are forced to be identical. It is not possible to measure the C and N contents using XEDS in the TEM. Therefore, only the composition of the primary solute elements (metal) is reported. The XEDS analyses of the nitrides confirmed their expected high Cr content. The experimental and calculated values presented in this table show that the average chromium depletion induced in the matrix during the ferritization treatment and as a consequence of nitride precipitation is low; the average chromium content of the as-welded $\alpha + M_2N$ (ferritic) regions is ~22.7 wt-% and the computed average chromium metallic fraction of the ferritic matrix is 22.3 wt-%. However, according to literature [11], narrow chromium depleted zones are established around chromium nitride precipitates, which can be strongly detrimental to localized corrosion resistance.

Figure 1 shows the calculated chromium, nickel and nitrogen composition profiles established in the overall microstructure after reheating treatments. As presented in Fig. 1a, intergranular γ_2 formed during the 1,200 °C isothermal anneal exhibited a heterogeneous chemical composition profile, which has been experimentally verified by the authors using XEDS microanalysis in the TEM [12]. This γ_2 is composed of an outer shell (next to the γ/α interface) enriched in Cr and N, and a core region (next to γ_1) depleted in these alloying elements. These unusual solute profiles are established due to the intergranular γ_2 growth during the high temperature isothermal anneal. The high diffusivity of the substitutional alloying elements at high temperatures makes this partitioning possible. However, during the cooling stage the limited diffusivity of the

Table 3 TEM measured chemical analysis (XEDS) and numerical calculations (NC) of the metallic fraction of the main elements in the ferritic matrix and nitrides in a ferritized sample (wt-%)

Phase		Fe	Cr	Ni
α	XEDS	70.4	24.0	4.6
	NC	72.85	22.3	4.84
M_2N	XEDS	8.8	89.9	0.18
	NC	2.4	97.6	0.05

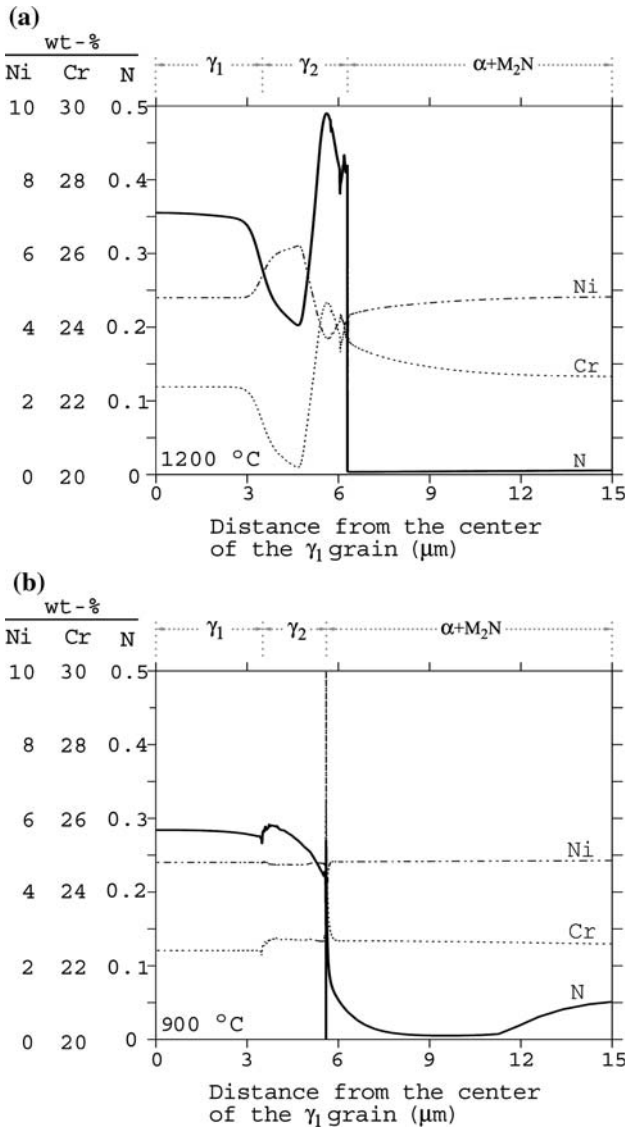

Fig. 1 Calculated alloy content across the system for samples reheated at 1,200 and 900 °C

substitutional elements leads to the occurrence of γ_2 growth with negligible substitutional solute partitioning with the parent ferrite.

In contrast to the solute partitioning observed as a result of the isothermal anneal at 1,200 °C, the γ_2 formed at 900 °C exhibits a nearly homogeneous chemical composition, as presented in Fig. 1b. The γ_2 formed at the lower temperature inherits the substitutional alloying concentration of the ferritic matrix due to low diffusivity of substitutional elements.

SEM and TEM analyses of nitride precipitation were in good agreement with numerical simulations. A considerable amount of chromium nitride precipitates were observed in ferritized as well as 900 °C reheated samples, whereas virtually no nitrides were observed in the 1,200 °C reheated samples. Figure 2 shows TEM micrographs of the general view of intragranular nitrides observed in a sample reheated to 900 °C. The intragranular nitrides varied in width between approximately 40 and 120 nm. Figure 2a shows a general view of a ferritic region containing Cr_2N nitrides (marked with arrows in the figure) and also some dislocations. In Fig. 2b, a selected area diffraction (SAD) pattern from the ferritic matrix, at the axis zone [011] α is shown. Figure 2c presents an enlarged detail of one of the nitrides in Fig. 2a; wider dark–bright contrast fringes inside nitrides can be seen, which correspond to Moiré patterns. A detailed crystallographic study of this nitride precipitation is presented in a previous work [6], where these nitrides were identified, by nano diffraction analysis, as trigonal Cr_2N.

Electrochemical experiments

Figure 3 shows the relationship between potential and current density established during the electrochemical pitting and DL-EPR experiments of HAZ microstructures. One representative curve of five tests is presented. In addition, Table 4 gives the average pitting potential and degree of sensitization (DOS) from the *potential–current density* curves. The lower corrosion resistance of HAZ microstructures compared to the wrought material is clearly evident. The pitting potential of the wrought material is 535 mV-SCE whereas the pitting potential of the HAZ microstructures is between 332 and 443 mV-SCE. Intense sensitization occurrence in the as-welded and in the 900 °C reheated HAZ microstructures was observed. On the other hand, the wrought and 1,200 °C reheated HAZ microstructures were not sensitized. One can additionally see in Table 4 a moderate increase in corrosion resistance after reheating treatments when compared to the ferritized samples. The occurrence of sensitization is explained by the SEM and TEM observations of Cr nitride precipitation and by the modeling results of nitrogen supersaturation in ferritic regions: the larger the nitrogen supersaturation in the ferritic regions, the larger the

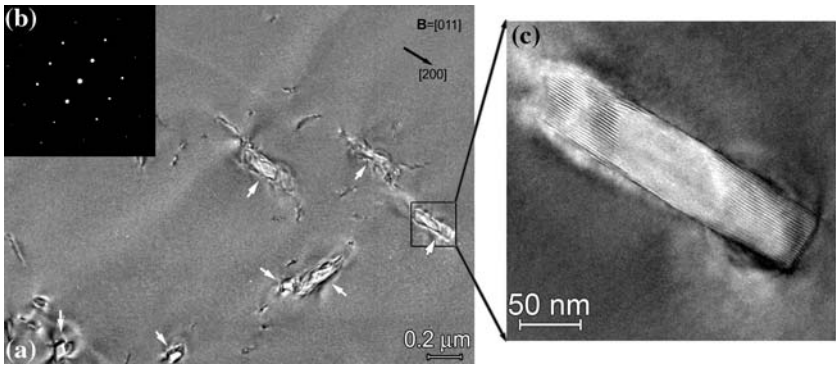

Fig. 2 TEM micrographs showing general view of nitride precipitation in a sample reheated at 900 °C. Wider dark–bright contrast fringes inside nitrides correspond to Moiré patterns

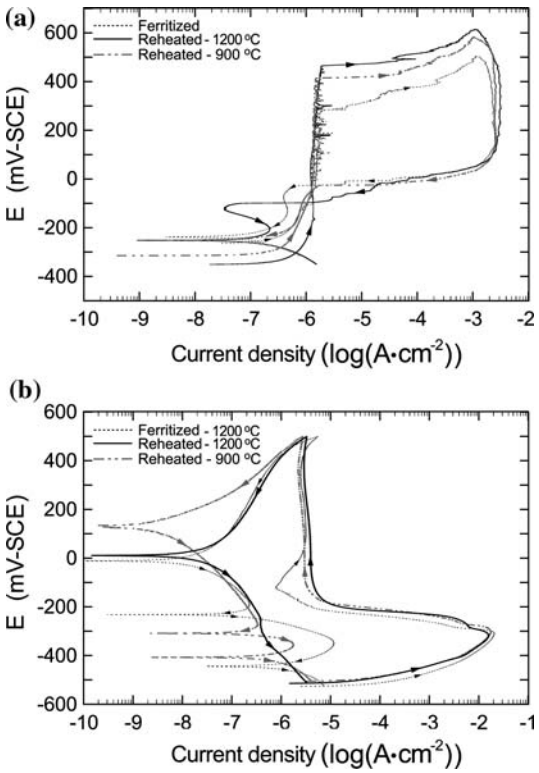

Fig. 3 Current density vs. Potential during pitting (**a**) and DL-EPR (**b**) electrochemical corrosion tests

Table 4 Pitting potential and degree of sensitization of the DSS UNS S32304 in the wrought condition, after ferritization and after reheating at 1,200 and 900 °C

Condition	Pitting potential (mV-SCE)	Degree of sensitization (dimensionless)
Wrought material	535 ± 52	0.0
Ferritized (1,350 °C)	332 ± 30	$8.4 \pm 1 \times 10^{-4}$
Reheated 1,200 °C	443 ± 30	0.0
900 °C	401 ± 27	$1.5 \pm 0.5 \times 10^{-4}$

sensitization due to Cr nitride precipitation. Detailed discussion is presented in "Analysis and discussion".

Figure 4 shows the surface appearance of the sample reheated at 900 °C after it has been subjected to the pitting corrosion tests. The sample surface appearance for all the other heat treatment conditions is similar to the one shown in Fig. 4. The largest part of the sample surface (almost 95%-area) was only slightly affected by the pitting

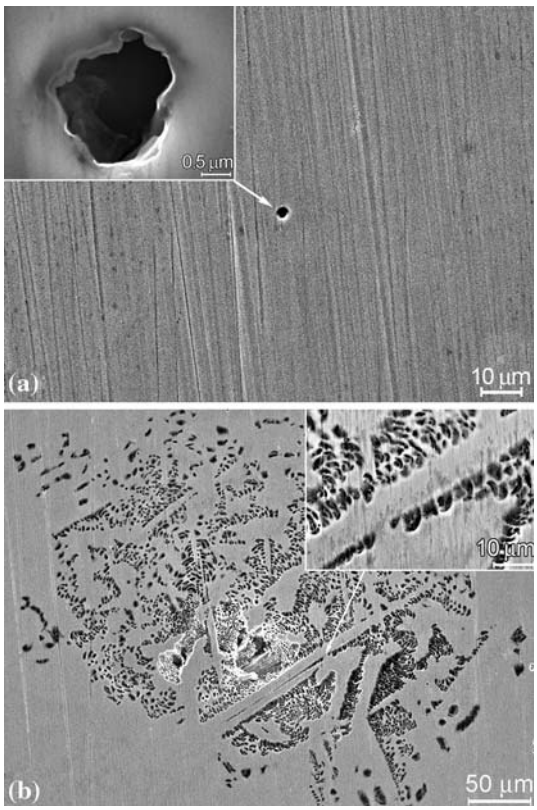

Fig. 4 SEM micrographs showing the surface appearance of sample reheated to 900 °C after being subjected to pitting corrosion electrochemical tests. (**a**) General appearance of the surface—which represents ~95% of the test surface-; (**b**) appearance of deeply damaged regions

corrosion test; in these regions (Fig. 4a) a low density, between approximately 50 and 200 pit·mm^{-2}, of small pits, between 1 and 3 μm in diameter, was observed. However, a few regions, with a number of regions per unit area ranging between approximately 0.15 and 0.35 region·mm^{-2},were observed that were severely corroded (Fig 4b). These regions, which varied in size from approximately 200–450 μm, consisted of a network of connected and unconnected pits of diverse sizes. Qualitatively, it was observed that the extent of damage in these regions followed the same order as the pitting potential: wrought material < 1,200 °C reheated < 900 °C reheated < ferritized.

Although it is not unambiguously clear, large side plates (possibly austenite) are evident at the sample surface of the corroded samples, Fig. 4b, that may possibly act as barriers to additional pitting damage. Aiming to further clarify the actual localization of pit-corrode regions among ferrite or austenite regions in microstructure, a sample reheated at 1,200 °C was electrolytic-etched after being submitted to pitting corrosion test. Figure 5 shows the appearance of that sample reheated at 1,200 °C after the pitting corrosion test followed by electrolytic etching. Although the electrolytic etching significantly modifies the prior appearance of the surface subjected to pitting test, it can be seen that pit-damaged regions were inside prior ferritic grains. As can be seen in this figure, the coarse intergranular allotriomorphic austenite and intragranular austenite regions acted as barriers for the growth of pitting damage. The detail presented on the top right of Fig. 5 shows the barrier effect of these austenite particles.

Figure 6 shows the appearance of the sample surface after DL-EPR tests. Corrosion attack of the sensitized areas in the ferritized sample as well as the one reheated at 900 °C occurred, but no such attach was observed in the 1,200 °C reheated samples. Corrosion attack during DL-EPR tests was mainly observed in two locations: (i) the middle region of ferritic grains where intense chromium nitride precipitation is expected and (ii) the near region of some γ/α interfaces, where chromium nitride precipitation is also expected, as previously discussed. The superior localized corrosion resistance of both γ_1 and γ_2 grains was observed.

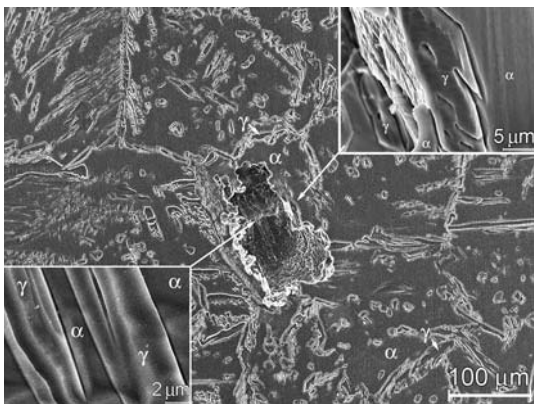

Fig. 5 SEM micrographs showing the appearance of the sample surface after pitting electrochemical corrosion test pursued by electrolytic etching. Sample reheated to 1,200 °C

The effect of alloying redistribution on the computed PRE index profiles

Figure 7 shows the calculated pitting resistance equivalent index (PRE = wt-% Cr + 3.3 wt-% Mo + 16wt-%N) profiles, established in the overall microstructure after reheating treatments. Aiming to simplify the kinetic computing simulations, which computing time strongly increases as a consequence of increasing the number of alloying elements included in the system, the molybdenum content was not used in the PRE computations. This simplification should exert a minor effect on the overall results because, (i) the Mo-content of the alloy is low (0.3 wt-%) and (ii) prior thermodynamic simulations (not presented) shown atomic partitioning of this element in microstructure contributes to PRE differences in a minor extent when compared to the effect of Cr- and N-content. In addition, only the elements in solid solution within the ferrite and austenite were taken into consideration to compute the PRE index profiles, i.e. the elements present in the form of M_2N where not taken into account.

The most significant aspect regarding the PRE index profiles (Fig. 7) is the low PRE index (22.3) of ferritic regions in the as-welded high temperature HAZ microstructures (ferritized samples) compared to the wrought material. In the wrought material the PRE index of α and γ are 25.3 and 23.1, respectively. On the other hand, the PRE index of reheated high temperature HAZ microstructures varies between 21.8 and 22.6 for α and 23.5 and 32.7 for γ. This reduction in PRE index suffered by ferritic regions, as a consequence of the welding thermal cycles, is mainly due to the almost absence of chromium partitioning between the austenitic ($\gamma_1 + \gamma_2$) and ferritic grains in the HAZ microstructures. This behavior is quite different to the observed in the wrought material, where the carefully selected combination of chemical composition and solubilization heat treatment results on an almost balanced PRE index between the two phases. Care should be taken because the reported PRE reduction within the ferritic regions ($\alpha + M_2N$) has not taken into account the localized Cr depletions around M_2N precipitates, which will have a strong influence on the localized corrosion resistance of such microstructures.

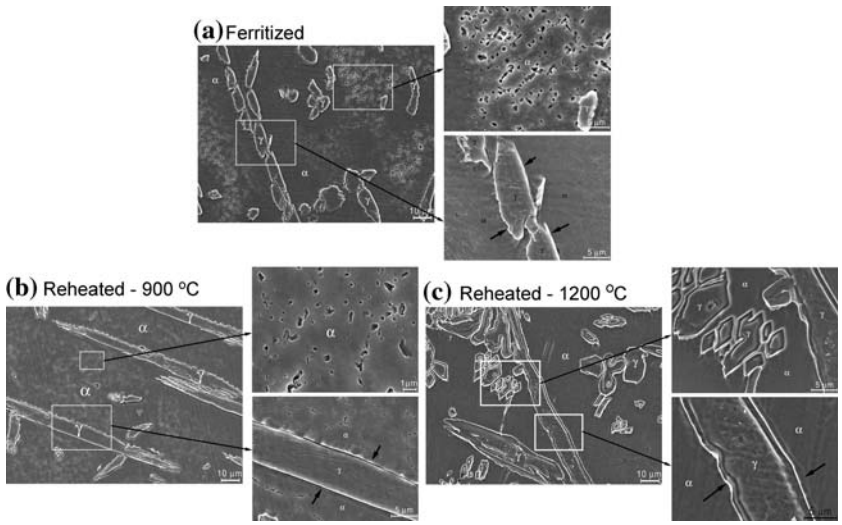

Fig. 6 SEM micrographs showing the appearance of the sample surface after DL-EPR electrochemical corrosion tests of (**a**) ferritized, (**b**) reheated to 900 °C, and (**c**) reheated to 1,200 °C samples

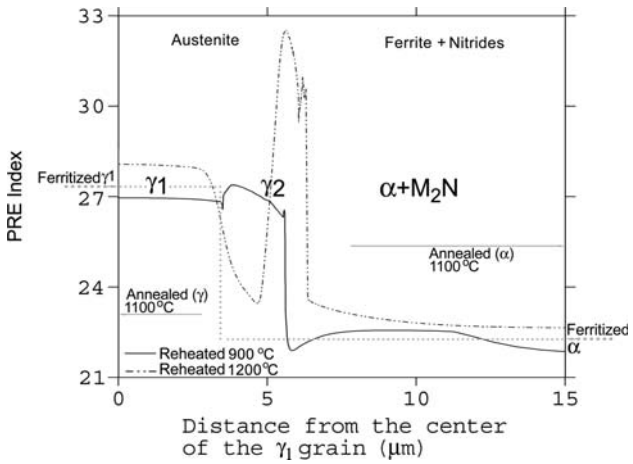

Fig. 7 Calculated PRE index profiles across the system for samples reheated at 1,200 and 900 °C. In the general PRE index equation (PRE = wt-% Cr + 3.3 wt-% Mo + 16wt-%N) the Mo-content effect was disregarded

The PRE index was developed to predict the overall pitting corrosion resistance of stainless steels in chloride solutions and this does not necessary predict the corrosion resistance in neither other solutions nor the differences of corrosion resistance inside microstructure among different constituents. Despite of this, in the next "Analysis and discussion", it is observed that the computed PRE-index profiles are a helpful tool to qualitatively describe the results of SEM analysis of the appearance of the sample surface after electrochemical experiments.

Analysis and discussion

The composition profiles calculated in this work for alloy UNS S32304, which technically is a Mo-lean alloy, should not be extrapolated to other duplex stainless steels as UNS S32205 or UNS S32750 because the effect of Mo on the thermodynamics and kinetics of those systems have not been evaluated in the present research. However, the present results can be used with care to evaluate previously reported results on the intragranular γ_2 precipitation and its effect on the corrosion resistance of DSS. In the case of intragranular γ_2, the nucleation of new austenite particles precedes austenite growth. Previous work has indicated several possible nucleation mechanisms for such new particles [2, 6, 7]. Among these mechanisms is heterogeneous austenite nucleation on dissolving nitrides [6, 7] and inclusions [2], which is more important in weld metal. In addition, sympathetic nucleation has been suggested [2]. Disregarding the nucleation mechanism, the growth of intragranular γ_2 will have some differences with respect to the growth of intergranular γ_2. One of the most important differences can be the abundant supply of nitrogen and chromium within the dissolving nitride colony where the intragranular γ_2 particles are growing. However, the much larger diffusivity of nitrogen compared to chromium suggest that Cr diffusion can be the controlling factor on intragranular γ_2 growth. Therefore, the high chromium content within this changing colony should play an important role on the acicular morphology of these particles.

In addition to the previously described differences between intergranular and intragranular γ_2 growth, there are some relevant similarities that should be mentioned. These similarities include the apparent controlling effect of chromium diffusion and the inhomogeneous composition profile along $\gamma_1/\gamma_2/\alpha$ "interfaces". It has been previously reported experimental evidence of such chemical inhomogeneity along $\gamma_1/\gamma_2/\alpha$ "interfaces" on very small prior-intragranular γ_1 that precipitated within nitrides colonies,

which grows as γ_2 within these changing nitride colonies during reheating treatments [7]. Therefore, these similarities strongly suggest that the results here presented for intergranular γ_2 growth can be a reasonable approximation to intragranular γ_2 growth and of course to its effects on the corrosion resistance of UNS S32304 DSS. Further research, including numerical simulation is necessary to clarify these similarities. However, the simulation of intragranular γ_2 nucleation and growth requires more elaborated models and one dimension approximations as the ones used here to model intergranular γ_2 growth may not be considered satisfactory.

The calculated chemical profiles presented in Fig. 1 do not fully agree with previously reported results on the chemical composition of intragranular γ_2 on super-duplex stainless steels with additions of Cu and W [8, 9]. On the other hand, the predicted and measured [12] composition profiles support corrosion resistance results for DSS UNS S13803 [14], which exhibits a similar chemical composition to the studied alloy UNS S32304. However, in addition to the differences in chemical composition of the Superduplex alloys with Cu and W additions, the calculations presented here are based on more elaborate kinetics models, which are expected to better represent the system. However, the simplifications here used include the reduction of the system to one dimension and the isothermal treatments. Thus, important differences with actual welds may be expected, especially for Superduplex alloys. Nevertheless, this new contribution helps to better understand the chemical partitioning among ferrite and austenite in duplex stainless steels and particularly its effects on corrosion resistance.

The PRE index of ferritic regions among the different HAZ microstructures, namely as-welded HAZ (ferritized samples) and reheated-HAZ (1,200 and 900 °C reheated samples), suffered only minor variations. However, the nitrogen content within the ferrite, and thus the fraction of chromium nitrides precipitated in this phase, underwent large changes. These changes have an important effect on the corrosion resistance of such microstructures. The predicted supersaturation of ferritic regions with nitrogen in the as-welded HAZ microstructure, which results in abundant intragranular M_2N precipitation, was reduced after reheating treatments. The 900 °C reheating treatment induced a moderate nitrogen content reduction in the ferritic regions near to the growing austenite, as shown in Fig. 1b. However, the ferritic region immediately adjacent to the α/γ_2 interface underwent an important nitrogen enrichment, which explains the previously reported nitride (M_2N) precipitation at the α/γ interface [6]. On the other hand, the 1,200 °C reheating treatment induced an almost complete exhaustion of nitrogen from ferritic regions. In both cases, a large amount or almost all the M_2N nitrides that formed within nitrogen supersaturated ferrite during the fast cooling following the ferritization treatment, dissolved during the reheating treatments and the nitrogen is incorporated by the growing austenite. The long diffusion paths during reheating at high temperatures allow for the nitrogen to be mostly incorporated by preexisting austenite particles that are growing, resulting in nitride-free ferrite, as verified by the presented calculation. On the other hand, the shorter diffusion paths experienced at lower temperatures favor a modest growth of preexisting austenite particles and the formation of acicular-type intragranular γ_2 colonies within the preexisting nitrides colonies that were far apart from austenite particles [7].

The superior localized corrosion resistance of both γ_1 and γ_2 grains was observed, even for the 1,200 °C reheating treatments in which relatively low PRE index value in the middle of γ_2 grains was predicted (Fig. 7). This result agrees with reported research on DSS UNS S31803 [14]. Besides localized corrosion occurrence in sensitized areas, DL-EPR test leads to generalized corrosion [15]. The extent of localized corrosion at phase interfaces was different in the diverse HAZ microstructures (Fig. 6). In the ferritized samples as well as the 900 °C reheated samples the corroded regions adjacent to the phase interfaces were narrow, contrary to the 1,200 °C reheated samples in which this corrosion damage occurred along a broader region around to the interface. This is probably due to occurrence of galvanic effects between α and γ grains, which have different Cr- and Ni-content in the near interface region (Fig. 1). The largest difference in Cr- and Ni-content in the near interface region between α and γ was in the 1,200 °C reheated samples (see Fig. 1), which were the samples displaying the broadest corrosion at phase interfaces. One can also see in Fig. 6 that some intragranular austenitic grains can be detached from the ferritic matrix as a consequence of phase interface corrosion, which is due to the above pointed out galvanic effect, as well as the large surface/volume ratio and small size of these γ particles. Thus, this small intragranular austenite particles detachment from the sample will worsen the corrosion damage in the material. This can be the mechanism behind the previously reported damaging effect of intragranular γ_2 on the corrosion resistance of duplex stainless steels. However, more research in different duplex alloys will be necessary to generalize this mechanism.

Summarizing, the numerical simulation and experimental results revealed that the moderately low PRE index established in ferritic regions of welded DSS UNS S32304 is the main cause for lower localized corrosion resistance of HAZ microstructures when compared with the wrought material. In addition, it can be also inferred that chromium nitride precipitation within ferritic regions further impairs the corrosion resistance of HAZ microstructures due to sensitization occurrence.

Thus, selective corrosion inside gamma grains, γ_1 and γ_2, is not the main cause for the poor corrosion resistance of DSS UNS S32304 HAZ microstructures. However, the fraction of chromium nitrides within the ferritic regions indirectly depends on the total fraction of austenite ($\gamma_1 + \gamma_2$), as austenite grains exhaust the nitrogen from the ferritic regions. In addition, at high reheating temperatures, the nitrides modify the substitutional alloy content profiles in the region near to the γ/α interfaces.

Precipitation of austenite displaying superior PRE index in the region adjacent to the γ/α interfaces when compared with ferrite can deteriorate the generalized corrosion resistance of HAZ microstructures due to galvanic effects. This effect should be particularly important in regions where profuse precipitation of small intragranular austenite particles occurs. In this case ferrite around these γ particles can be easily damaged due to both the large surface/volume ratio of γ particles and their small size.

Conclusions

The results and analyses from the calculations and experimental measurements on heat-treated DSS UNS S32304 have led to the following conclusions:

- The electrochemical pitting and DL-EPR tests showed an impaired corrosion resistance of HAZ microstructures with respect to the wrought material. This reduction of corrosion resistance after welding was mainly attributed to a decrease in the corrosion resistance of the HAZ ferritic grains. This was attributed to (i) the mean chromium content of these ferritic grains is the same chromium content of the alloy (i.e. ferritic grains in the HAZ exhibited lower chromium content than ferritic grains in the wrought material) and (ii) the presence of chromium depleted regions around nitrides, which were often observed.
- As-welded HAZ microstructures displayed lower localized corrosion resistance and higher degree of sensitization than reheated HAZ microstructures. The extent of corrosion resistance improvement after reheating treatment was mainly caused by the removal of nitrogen from ferritic regions, which occurred as a consequence of γ_2 growth.
- The observed corrosion resistance improvement was more pronounced after isothermal reheating to 1,200 °C, compared to the 900 °C reheating treatment, which appears to be directly related to the removal of nitrogen within the ferrite grains.
- In contrast with what has been reported in literature for superduplex stainless steels [2, 3], a direct detrimental effect of intergranular γ_2 precipitation on corrosion resistance was not observed. Selective corrosion inside gamma grains, γ_1 and γ_2, was not the main cause for the impaired corrosion resistance of DSS UNS S32304 HAZ microstructures. However, the observed ferritic matrix dissolution around intragranular γ_2 suggest that small gamma particles detachment from the material is the probable cause for a high corrosion rate.

Acknowledgments The authors would like to acknowledge to LNLS and FAPESP, for funding the actual and predecessor projects.

References

1. Ogawa TO, Koseki T (1989) Weld J 68:181
2. Atamert S, King JE (1991) Z Metallkd 82:230
3. Nilsson JO, Karlsson L, Andersson JO (1995) Mat Sci Techn 11:276
4. Gooch TG (1996) Weld J 75:135
5. Gregory A, Nilsson J-O (2002) Met Mat Trans – A 33A:1009
6. Ramirez AJ, Lippold JC, Brandi SD (2003) Met Mat Trans – A 34A:1575
7. Ramirez AJ, Ph.D. Thesis, University of São Paulo, São Paulo, Brazil, 2001, p. 241. Full text available at http://www.teses.usp.br/teses/disponiveis/3/3133/tde–02012002–175418/
8. Hertman S, Huhtala T, Karlsson L, Nilsson J-O, Jargelius-Pettersson R, Wilson A (1997) Mater Sci Tech 13:604
9. Nilsson J-O, Huhtala T, Jonsson P, Karlsson L, Wilson A (1996) Met Mat Trans – A 27A:2196
10. Majidi AP, Streicher MA (1984) Corrosion 40:393
11. Andersson JO, Helander T, Hoglund LH, Shi PF, Sundman B (2002) CALPHAD 26:273
12. Garzón CM, Ramirez AJ (2006) Acta Mater 54:3321
13. Andersson JO, Ågren J (1992) J Appl Phys 72:1350
14. Muthupandi V, Bala Srinivasan P, Seshadri SK, Sundaresan S (2004) Sci Technol Weld Joi 9:47
15. Menendez H, Devine TM (1990) Corrosion 46:410